

# Phase development in pulsed laser deposited $\text{Pb}[\text{Yb}_{1/2}\text{Nb}_{1/2}]\text{O}_3\text{-PbTiO}_3$ thin films

V. Bornand\*, S. Trolier-Mckinstry

The Pennsylvania State University, Department of Materials Science and Engineering, Materials Research Laboratory, University Park, PA 16802-4801, USA

Received 10 August 1999; received in revised form 16 February 2000; accepted 16 February 2000

## Abstract

$(1-x)\text{Pb}[\text{Yb}_{1/2}\text{Nb}_{1/2}]\text{O}_3-x\text{PbTiO}_3$  (PYbN-PT,  $x = 0.4$  and  $0.5$ ) /  $\text{SrRuO}_3$  (SRO) heterostructures have been prepared by pulsed laser deposition (PLD) on  $\langle 100 \rangle_{\text{pc}}$ -oriented  $\text{LaAlO}_3$  (LAO) substrates (the subscript pc refers here to the pseudo-cubic perovskite subcell). Careful control of both lead volatilization and pyrochlore formation during the growth appears to be essential to obtain perovskite PYbN-PT thin films with good crystalline, electrical and ferroelectric properties. By utilizing PbO-enriched ceramic targets and adjusting deposition parameters such as the laser frequency, the chamber pressure, the target to substrate distance and/or the substrate temperature, high-quality thin films can be successfully grown with a single out-of-plane  $\langle 001 \rangle_{\text{pc}}$  orientation and an in-plane heteroepitaxial arrangement of  $[110]_{\text{pc}}$  PYbN-PT //  $[110]_{\text{pc}}$   $\text{SrRuO}_3$ . When processed in the 560–660°C temperature range, with a dynamic  $\text{O}_3/\text{O}_2$  pressure of 300–400 mTorr and relatively high laser repetition rates, PYbN-PT films exhibit improved ferroelectric properties. The typical values of the remanent ( $P_r$ ) and saturation ( $P_s$ ) polarizations increase up to 50 and 80  $\mu\text{C}/\text{cm}^2$ , respectively. © 2000 Published by Elsevier Science S.A. All rights reserved.

**Keywords:** Laser ablation; Ferroelectric thin film heterostructures; Epitaxy; Lead ytterbium niobate - lead titanate

## 1. Introduction

Ferroelectric films can display a wide range of dielectric, ferroelectric, piezoelectric, electrostrictive and pyroelectric characteristics [1,2]. The potential utilization of these properties in a new generation of devices has motivated intensive studies on the synthesis, characterization and processing-microstructure-property relationships of such films during the past 20 years. In particular, advances in ferroelectric and piezoelectric thin film deposition technology have generated a considerable interest within the electronic materials community. Originally directed towards memory applications it is now rapidly spreading to other areas such as the biomedical, automotive, computer and communication industries [3–6].

Many ferroelectric materials under research for thin film microelectromechanical systems (MEMS) are perovskite compounds, such as the morphotropic phase boundary  $\text{Pb}[\text{Zr}_{1-x}\text{Ti}_x]\text{O}_3$  (PZT) [7]. Though successful devices using PZT have already been demonstrated, the piezoelectric properties at best approach those of hard PZT ceramics.

Substrate clamping and reduction of the extrinsic contributions to the piezoelectric coefficients are, at least in part, responsible for the disparities between bulk ceramic and thin film characteristics [8,9]. Given the property limitations of PZT thin films, alternatives, including  $\text{Pb}[\text{B}'\text{B}'']\text{O}_3$  and  $(1-x)\text{Pb}[\text{B}'\text{B}'']\text{O}_3-x\text{PbTiO}_3$  materials, are particularly interesting [10,11]. The large polarization and permittivity values of such complex perovskites make them promising candidates for microelectromechanical systems. Important relaxor systems which show enhanced piezoelectric activity are  $(1-x)\text{Pb}[\text{Zn}_{1/3}\text{Nb}_{2/3}]\text{O}_3-x\text{PbTiO}_3$  (PZN-PT) [12] and  $(1-x)\text{Pb}[\text{Mg}_{1/3}\text{Nb}_{2/3}]\text{O}_3-x\text{PbTiO}_3$  (PMN-PT) [13]. As shown by Park et al. [13,14], large piezoelectric coefficients (in excess of 2500 pC/N) can be observed along the  $\langle 001 \rangle$ -direction in rhombohedral single crystals. Similarly,  $\langle 001 \rangle$  heteroepitaxial PMN-PT films deposited on  $\text{SrRuO}_3$  /  $\text{LaAlO}_3$  substrates also show enhanced piezoelectric coefficients relative to PZT films of the same thickness [15,16]. For MEMS, the major challenge is to prepare these materials as 'single crystal' epitaxial thin films between metallic electrodes and integrate them so that their ferroelectric and electromechanical properties can be used in piezoelectric devices.

When dealing with ferroelectric MEMS, both the choice

\* Corresponding author. Tel.: +33-467-14-33-43; fax: +33-467-14-42-90.

E-mail address: vbornand@lpmc.univ-montp2.fr (V. Bornand).

Table 1  
SrRuO<sub>3</sub> and PYbN-PT growth parameters for pulsed laser deposition

Parameters	SrRuO <sub>3</sub> [21]	(1 - x) PYbN-x PT
Temperature (°C)	680	560–680
Atmosphere	10% O <sub>3</sub> -90% O <sub>2</sub>	10% O <sub>3</sub> -90% O <sub>2</sub>
Pressure (mTorr)	200	100–400
Laser power (mJ)	250	250
Laser fluence (J/cm <sup>2</sup> )	2.5	2.5
Laser frequency (Hz)	18	12–20
Target	Stoichiometric	25 wt.% excess PbO x=0.4–0.5
Target to substrate distance (cm)	6.5	4.5–7

of the ferroelectric relaxor and the bottom electrode are important, as the quality of many electronic heterostructures ultimately rely upon the structural and electrical characteristics of the underlying electrode. The electrode material should possess a good conductivity, a smooth surface and good adhesion, in addition to an epitaxial match to the substrate and the ferroelectric [17,18]. Moreover, the bottom electrode should be thermally stable in oxidizing ambients at high temperatures, as the ferroelectric materials generally crystallize through high-temperature oxygen-based processes. Given this, SrRuO<sub>3</sub> (SRO) was chosen as the bottom electrode [19–21].

In the present study, we undertook to prepare phase-pure oriented and heteroepitaxial thin films of lead ytterbium niobate - lead titanate (1 - x) Pb[Yb<sub>1/2</sub>Nb<sub>1/2</sub>]O<sub>3</sub> - x PbTiO<sub>3</sub> (PYbN-PT) on heteroepitaxial strontium ruthenate metallic oxide bottom electrodes. Of particular interest was their morphology and crystallinity as a function of the deposition conditions. The high Curie point (~360°C) of lead ytterbium niobate-based materials at the morphotropic phase boundary (x ~ 0.5) should greatly improve the high temperature capabilities of piezoelectric MEMS relative to lead magnesium niobate-based compounds. Although some research has been reported on the synthesis and characterization of PYbN-PT bulk ceramics [22,23], there is no literature on thin films to date.

Pulsed laser deposition (PLD) was used to grow the films since it enables a rapid turn around time for new compositions. Our research efforts were focused on the investigation of processing-composition-microstructure-property relationships of PYbN-PT / SRO heterostructures. Two nominal compositions (1 - x) Pb[Yb<sub>1/2</sub>Nb<sub>1/2</sub>]O<sub>3</sub> - x PbTiO<sub>3</sub> were studied, x = 0.5 and x = 0.4, lying at the morphotropic phase boundary and to the pseudo-cubic side, respectively.

## 2. Experimental procedure

(1 - x) Pb[Yb<sub>1/2</sub>Nb<sub>1/2</sub>]O<sub>3</sub> - x PbTiO<sub>3</sub> (PYbN-PT) / SrRuO<sub>3</sub> (SRO) heterostructures were deposited on <100><sub>pc</sub>-oriented LaAlO<sub>3</sub> (LAO) substrates by pulsed laser deposition using a KrF excimer laser operating at 248 nm. This

technique is an excellent method for the deposition of thin film perovskite materials [24] because of its simplicity, versatility and comparatively good transfer of the target composition to the film. The specific processing conditions for both materials are summarized in Table 1. More details on the SrRuO<sub>3</sub> deposition are given elsewhere [21]. The incident laser beam was focused at an angle of 45° onto the targets [25] with a constant pulse energy density of 2.5 J/cm<sup>2</sup> and repetition rates varying from 12 to 20 Hz. To reduce non-uniform erosion as well as droplet formation, the targets were rotated during the whole ablation process. Growth temperatures between 560 and 680°C were achieved by adhering the substrates, with silver paint, to a stainless steel block-style heater placed opposite and parallel to the target (on-axis deposition configuration). Before each experiment, the substrates were cleaned ultrasonically using Micro Lab Solvent, deionized water, acetone and ethanol, sequentially. Film depositions were performed in a dynamic 100–400 mTorr pressure of a mixture of 10% O<sub>3</sub> - 90% O<sub>2</sub>, the 10% O<sub>3</sub> atmosphere referring to the undistilled output of a commercially available ozone generator. In good agreement with previous work, an oxidizing environment during the deposition process helped to form and stabilize the desired perovskite phase at the deposition temperatures while the presence of ozone allowed a better control of Pb and PbO<sub>x</sub> phases volatilization [25]. Immediately after deposition, the samples were cooled, under the same pressure and in the same atmosphere O<sub>3</sub>/O<sub>2</sub> mix until 400°C, without additional annealing treatment.

The strontium ruthenate bottom electrode (350 nm-thick layer, typically) was ablated from a stoichiometric SrRuO<sub>3</sub> target purchased from Target Materials International. The low lattice mismatch, at room temperature, with LaAlO<sub>3</sub>

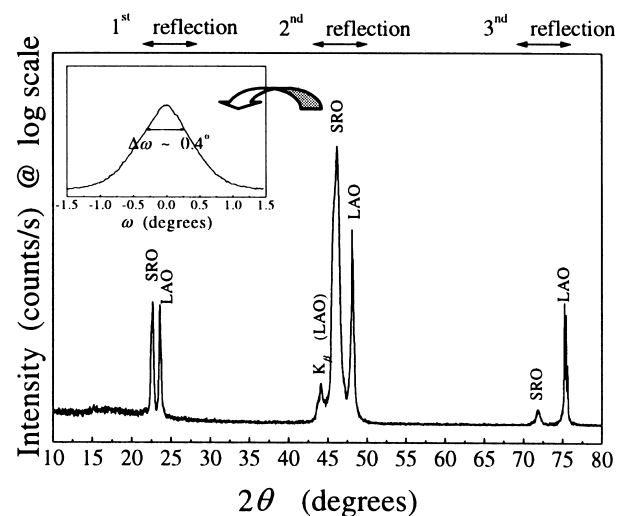


Fig. 1. X-ray diffraction  $\theta$ - $2\theta$  scan and (002)<sub>pc</sub> rocking curve insert of a SrRuO<sub>3</sub> thin film deposited on a (100)<sub>pc</sub> LaAlO<sub>3</sub> substrate. The peaks are indexed in the pseudo-cubic cell. Calculated lattice parameter for each phase:  $a_{\text{SRO}} = 3.92 \pm 0.01 \text{ \AA}$  ( $a_{\text{th}} = 3.930 \text{ \AA}$ );  $a_{\text{LAO}} = 3.79 \pm 0.01 \text{ \AA}$  ( $a_{\text{th}} = 3.795 \text{ \AA}$ ). (Process conditions are specified in Table 1).

( $\sim 3.55\%$  in the pseudo-cubic perovskite subcell) allowed the growth of strongly  $\langle 001 \rangle_{\text{pc}}$ -oriented SrRuO<sub>3</sub> layers on  $\langle 100 \rangle_{\text{pc}}$ -oriented LaAlO<sub>3</sub> substrates (Fig. 1). The lattice parameter  $a_{\text{pc}} \sim 3.93 \pm 0.01$  Å, calculated from XRD spectra, agrees with the theoretical value of the relaxed material ( $a_{\text{th}} \sim 3.93$  Å) suggesting that the as-grown bottom electrode is weakly - if not - stressed near the surface.

PYbN-PT films were then deposited using sintered ceramic targets with excess PbO. The  $(1-x)$  PYbN  $-x$  PT ( $x = 0.4$  and  $0.5$ ) solid solutions were prepared by a two-stage calcination technique starting from reagent grade powders of PbO, Yb<sub>2</sub>O<sub>3</sub>, Nb<sub>2</sub>O<sub>5</sub> and TiO<sub>2</sub> [26]. The wolframite method was followed [22], leading to phase pure perovskite PYbN-PT after calcination at 1200 and 750°C, respectively, without the appearance of stable pyrochlore phases detectable by X-ray diffraction (Fig. 2). It is well known in the PLD literature that Pb losses generally occur during the growth of Pb-based ferroelectric oxides [25]. It is generally believed that this is mainly due to the Pb evaporation from the hot substrate. Thus, to minimize and compensate for the expected PbO losses during the high-temperature PLD process, 25 wt.% excess PbO was added to the PYbN-PT powder before pellet formation and sintering at 850°C. By covering the pellets with a Pb-source during the temperature cycle, less than 1 wt.% loss occurs in the target.

PYbN-PT / SRO heterostructures were then characterized to determine the phase assemblage, crystalline quality, dielectric and ferroelectric properties. X-ray diffraction studies were performed by both  $\theta$ - $2\theta$  diffraction patterns and  $\omega$ -scans on a Scintag Pad V diffractometer (JSO-Debyelex 1001). In-plane texture was measured via  $\varphi$ -scans and X-ray pole figure analyses on a X'PERT Phillips four-circle diffractometer. Both devices were operated using the K $\alpha$  emission of a Cu anode and were equipped with graphite monochromators. The elemental composition and the morphology of the films were investigated by energy

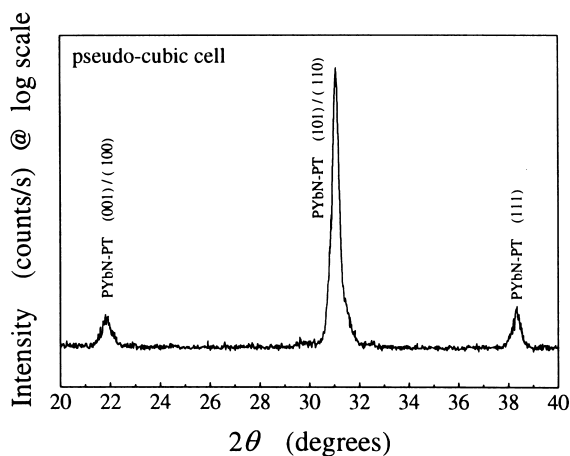


Fig. 2. X-ray diffraction  $\theta$ - $2\theta$  scan of a PYbN-PT (50/50) solid solution used for the target synthesis. The peaks are indexed in the pseudo-cubic cell.

dispersive spectroscopy (EDS) and surface/cross-sectional scanning electron microscopy (SEM), using a Hitachi S-3500 and a ISI-DS 130 dual stage electron microscope, respectively. Electrical measurements were performed through the film thickness using Pt dot electrodes of 0.3 mm in diameter sputtered through a shadow mask to the film surface. Ferroelectric measurements were made using a Radiant Technology RT66A standardized ferroelectric test system. The hysteresis loops presented have not been compensated for leakage currents.

### 3. Results and discussion

#### 3.1. Stabilization of the perovskite phase

The first step in the structural optimization of PYbN-PT thin films consisted of studying the film-growth environment in order to correlate deposition conditions with the stoichiometry, morphology, uniformity and crystallinity of the film. Thus, parameters such as the laser frequency, the chamber pressure, the substrate temperature and the target-to-substrate growth distance were varied to investigate their influence on the film quality. Some generalizations are then allowed, even though the complete interpretation is often complicated by the fact that the variation of a single factor may have ramifications on multiple aspects of the ablation process. For example, the ambient pressure and optimal target-to-substrate distance are interrelated. Due to the increased collisions between the laser-produced plume and the background gas, the plume dimension decreases as the background gas pressure increases. Therefore, the target-to-substrate distance may need to be changed to achieve the appropriate level of bombardment.

For PYbN-PT thin films deposited on SRO / LAO substrates, experiments have shown that stabilization of the perovskite material during growth requires reasonable deposition / growth rates, which necessitates high laser frequencies ( $f \geq 14$  Hz) and 300–400 mTorr of background O<sub>3</sub>/O<sub>2</sub> in the chamber during deposition. The best results were obtained when the samples were at the extremity of the plume (Fig. 3). Collisional scattering and broadening of the vapor plume at lower pressures lead to slower growth rates and Pb-deficient thin films while the higher evaporation rates associated with the lower repetition frequencies give rise to porous poor-quality layers. By keeping the laser fluence constant and increasing the repetition rate (i.e. decreasing the time between laser pulses), complete and continuous film formation can be achieved as a result of a high instantaneous vapor arrival. In these conditions, strongly  $\langle c \rangle$ -oriented thin films can be successfully grown due to the modest lattice mismatch between the two pseudo-cubic perovskite structures PYbN-PT and SRO ( $\sim 3.30\%$  at room temperature).

However, given this set of deposition conditions, control of the film structure and the degree of orientation are

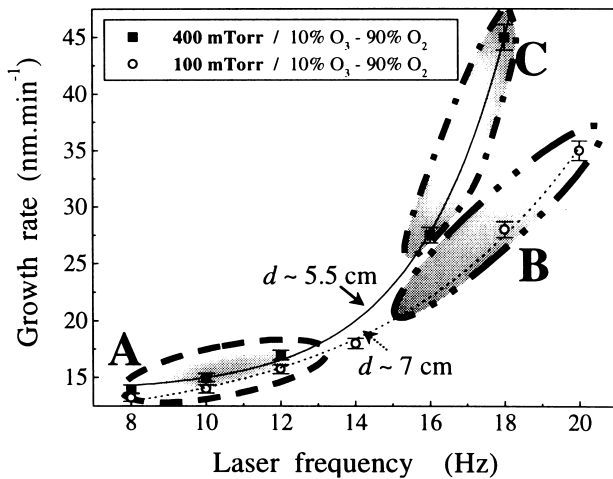


Fig. 3. Growth rate of PYbN-PT (50/50) thin films deposited on SRO / LAO substrates as a function of laser frequency and background  $O_3/O_2$  pressure. ( $T \sim 620^\circ\text{C}$ ; samples at the extremity of the plume.) (A) Parasitic phases predominant, (B) perovskite / parasitic phases mix, (C) perovskite phase region.

subjected to two additional parameters, the target to substrate distance (Fig. 4) and the substrate temperature (Fig. 5). In particular, the energetic and spatial distribution of the laser-generated flux greatly influences the film uniformity. The highly forward directed nature of the plume and subsequent interactions with the ambient gas give rise to a complex distribution of material and, as plotted on Fig. 4, the degree of orientation estimated through the Lotgering factor  $f(00l)$  (from normalized intensities) is maximum when the substrate is located at the extremity of the luminescent plasma. For shorter distances, irregular and rough morphologies are observed either due to high growth speeds associated with the strong plume confinement around the substrate or excessive bombardment of the substrate surface. The decrease in orientation for higher distances can be explained by a significant reduction of both the

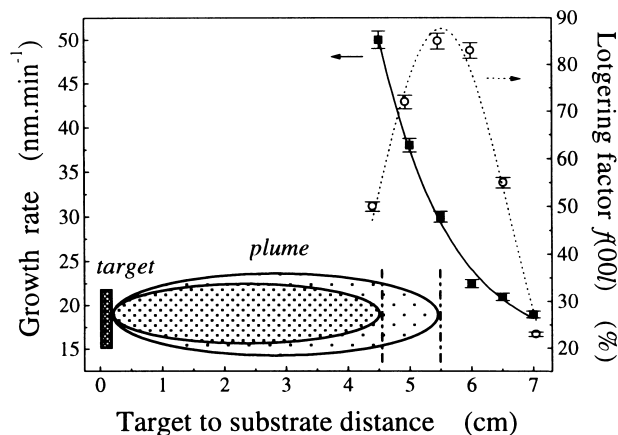


Fig. 4. Growth rate and degree of orientation along the  $\langle c \rangle_{pc}$ -direction of PYbN-PT (50/50) thin films deposited on SRO / LAO substrates as a function of target to substrate distance. ( $f \sim 16$  Hz;  $P \sim 300$  mTorr;  $T \sim 560^\circ\text{C}$ ).

concentration of ejected matter from the target that is transmitted to the substrate and the kinetic energy of the atomic species reaching the substrate. Apparently, for these growth temperatures, the additional atomic mobility associated with bombardment is insufficient to maintain heteroepitaxy. The presence of non-oriented material observed in such films is consistent with a random, secondary nucleation.

The effect of the substrate temperature appears to be more important in obtaining a particular crystal structure. It was found that temperatures between  $560$  and  $660^\circ\text{C}$  are necessary to nucleate the correct crystallographic phase and favor the growth of  $\langle c \rangle$ -oriented layers (Fig. 5). Lower temperatures reduce the surface diffusion coefficient of the adsorbed vapor atoms and, thus, their reactivity, limiting the formation of the equilibrium perovskite phase. Higher temperatures lead to volatilization of too much  $PbO$ , again limiting phase purity. In addition, the minimum temperature required for growth of perovskite  $(1-x)$  PYbN  $-x$  PT thin films with less than 2–3% of pyrochlore second phase is sensitive to the composition of the target and decreases from  $620$  to  $560^\circ\text{C}$  as  $x$  increases from  $0.4$  to  $0.5$ . The formation of the ferroelectric perovskite phase is enhanced as the  $PbTiO_3$  content ( $x$ ) increases. This agrees with the tolerance factor for the system [27].

### 3.2. Structural and microstructural analysis

Temperatures in the  $560$ – $660^\circ\text{C}$  window favor the growth of  $\langle c \rangle$ -axis perovskite normal to the substrate. XRD patterns with respect to the deposition temperature for PYbN-PT (60/40) / SRO / LAO heterostructures are shown in Fig. 6. It is clear that a strong preferential orientation with the  $\{001\}_{pc}$  PYbN-PT planes parallel to the  $\{001\}_{pc}$  SRO ones is stabilized. The crystal quality and degree of orientation of the films improve with temperature, while residual volumes of non-epitaxial perovskite and excess  $PbO_x$  or pyrochlore

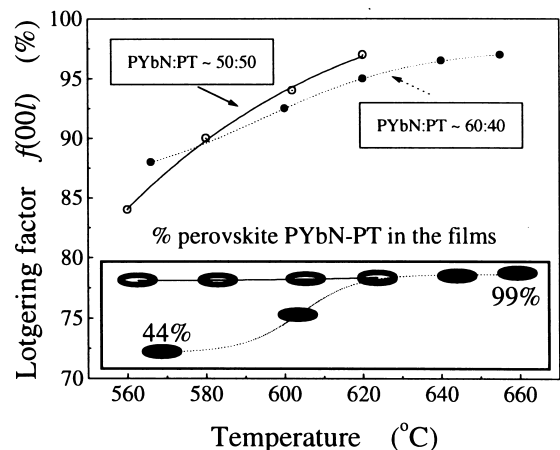


Fig. 5. Perovskite phase purity and degree of orientation along the  $\langle c \rangle_{pc}$ -direction of PYbN-PT thin films deposited on SRO / LAO substrates as a function of ceramic target composition and substrate temperature. ( $f \sim 16$  Hz;  $P \sim 300$  mTorr;  $d_{\text{target-substrate}} \sim 5.5$  cm). (○—) PYbN-PT (50/50) (●—) PYbN-PT (60/40).

phases are progressively removed. A little substrate misorientation or possible slight miscut explains why we observe different intensities of the diffraction peak of the substrate. Many phases (mainly pyrochlore ones) with nearly identical X-ray signatures and plausible stoichiometries exist, making very difficult an unambiguous assignment of the peak at  $2\theta \sim 34.30^\circ$ . However, the intensity of the diffraction peak from this oxygen or lead deficient pyrochlore phase decreases significantly with increasing temperatures,

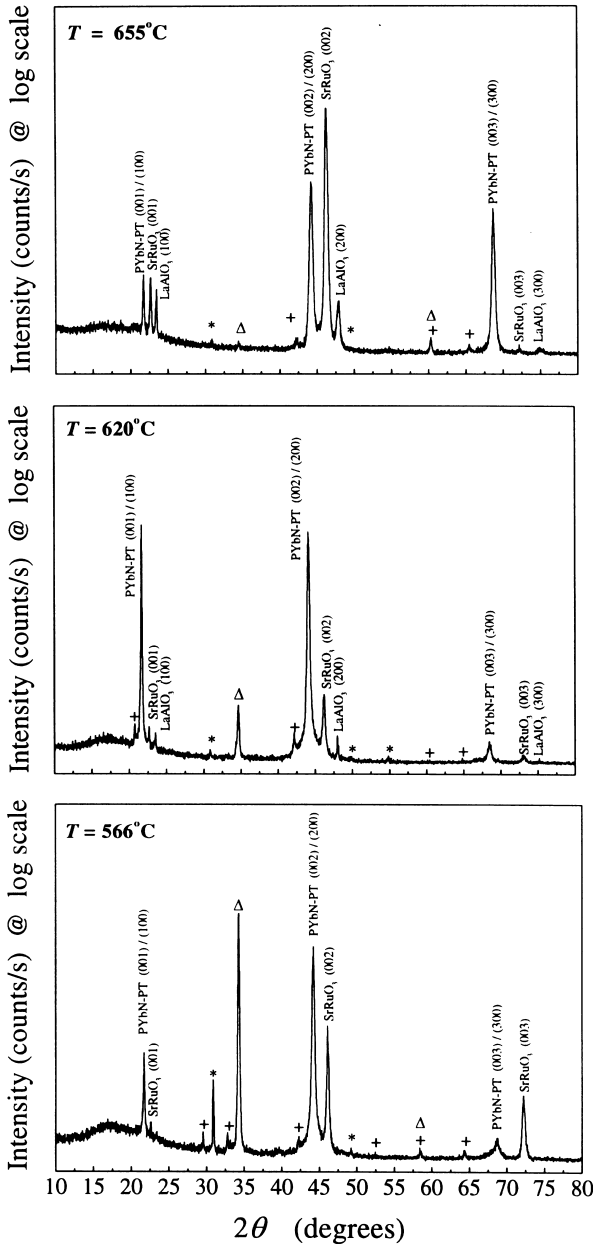


Fig. 6. X-ray diffraction  $\theta$ – $2\theta$  scans of PYbN-PT (60/40) thin films deposited on SRO / LAO substrates at increasing temperatures. The peaks are indexed in the pseudo-cubic cell. (\*) non-epitaxial PYbN-PT perovskite, ( $\Delta$ ) Pyrochlore, (+)  $\text{PbO}_x$ . ( $f \sim 16$  Hz;  $P \sim 300$  mTorr;  $d_{\text{target-substrate}} \sim 5.5$  cm).

indicating good phase purity within the resolution of the instrument (2%).

In order to investigate in more detail the crystallinity of the films and to determine the distribution profile of the pyrochlore phase in the layers, a sequential set of grazing incidence X-ray diffraction scans was performed with different incident angles. The use of low incidence angles significantly increases the path length of the incident and diffracted beams in the layers. Fig. 7 shows the results obtained on a 1.5  $\mu\text{m}$ -thick PYbN-PT (60/40) thin film previously deposited at  $566^\circ\text{C}$  on a SRO / LAO substrate. It is clear from the  $\alpha$  dependence of the pyrochlore peak that the second phase is concentrated near the bottom of the film. The pyrochlore formation and crystallization mostly occur during the first steps of the nucleation / growth process for low-temperature depositions. Higher deposition temperatures enhance the stability of the perovskite structure and can thus help to limit, indeed suppress, the formation of this non-ferroelectric phase. If  $\text{PbO}_x$  traces still remain for temperatures higher than  $600^\circ\text{C}$  (typically  $<1$  vol.%), diffraction peaks from other phases are not observed, suggesting the absence of any significant chemical reactions at the interface. The formation of the oriented ferroelectric perovskite material may be favored by the presence of a suitable structural and chemical template, i.e. the (001)<sub>pc</sub> surface of the  $\langle c \rangle$ -axis oriented  $\text{SrRuO}_3$  bottom electrode.

The heterostructures show some roughness due to the well-defined columnar microstructures associated with the laser deposition process (Fig. 8). Very little, if any, intermixing between the different layers can be distinguished. In the studied temperature range, the thermal energy that the condensing species attain at the substrate surface allows for increased surface mobility and energy for preferred nucleation and  $\langle c \rangle$ -oriented growth on the lattice-matched SRO layer. It appears that in most cases, the amount of excess PbO supplied to the films was sufficient to overcome PbO

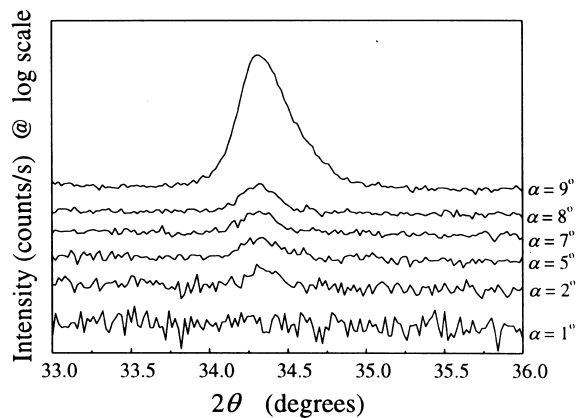


Fig. 7. Grazing incidence X-ray diffraction scans of a PYbN-PT (60/40) thin film deposited on a SRO / LAO substrate heated at  $566^\circ\text{C}$ . ( $f \sim 16$  Hz;  $P \sim 300$  mTorr;  $d_{\text{target-substrate}} \sim 5.5$  cm). The scans have been taken at different X-ray incidence angle ( $\alpha$ ) which correspond to different penetration depths.

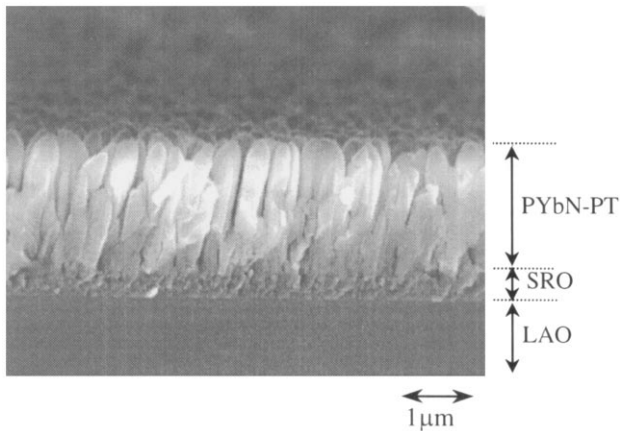


Fig. 8. SEM of the cross-section of a 1.8  $\mu\text{m}$ -thick PYbN-PT (60/40) thin film deposited on a SRO/LAO substrate heated at 655°C. ( $f \sim 16$  Hz;  $P \sim 300$  mTorr;  $d_{\text{target-substrate}} \sim 5.5$  cm).

volatilization problems which might lead to Pb-deficient layers. EDS analyses show that, within the 560–660°C temperature range, the composition of the PYbN-PT thin films is close to the nominal stoichiometry.

Rocking curve analyses are consistent with improved crystallinity when the temperature is increased (Fig. 9). The rather low values of the full width at half maximum (FWHM) demonstrate the good crystalline quality of the as-grown PYbN-PT thin films. For the same geometry, the SRO bottom electrode and LAO substrate have a 0.4 and 0.3° FWHM, respectively. Finally, texture determinations confirm the heteroepitaxial growth of the films. Fig. 10 shows the X-ray diffraction azimuthal  $\varphi$ -scan of the (110) reflection for a PYbN-PT (60/40) thin film deposited at 655°C on a SRO/LAO substrate. The four-fold symmetry and the fact that significant intensities are only observed at  $\varphi = 0, 90, 180,$  and  $270^\circ$  clearly indicate that the film is

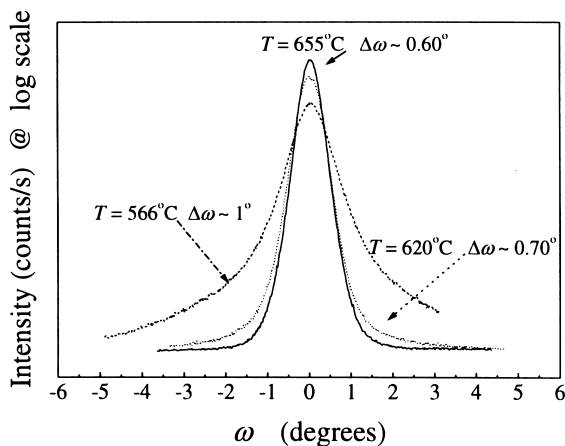


Fig. 9. Rocking curves of the (002)<sub>pc</sub> reflection of PYbN-PT (60/40) thin films deposited on SRO/LAO substrates at increasing temperatures. ( $f \sim 16$  Hz;  $P \sim 300$  mTorr;  $d_{\text{target-substrate}} \sim 5.5$  cm.)

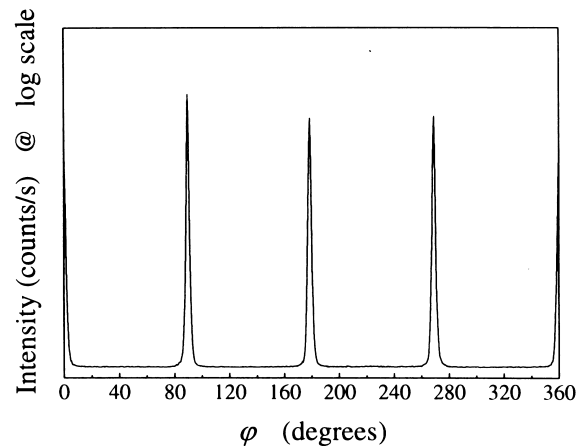


Fig. 10. X-ray diffraction  $\varphi$ -scan of the (110)<sub>pc</sub> reflection ( $2\theta \sim 31.078^\circ$ ) of a typical heteroepitaxial PYbN-PT (60/40) thin film deposited on a SRO/LAO substrate heated at 655°C. ( $f \sim 16$  Hz;  $P \sim 300$  mTorr;  $d_{\text{target-substrate}} \sim 5.5$  cm). ( $0 \leq \varphi \leq 360^\circ$ ;  $\Delta\varphi = 0.5^\circ$ ;  $\chi = 45.75^\circ$ ).

single domain with the in-plane  $[110]_{\text{pc}}$  PYbN-PT //  $[110]_{\text{pc}}$  SRO heteroepitaxial arrangement. The absence of any detectable peaks between these four major ones demonstrates the absence of any misoriented grains. The associated  $\Delta\varphi$  FWHM of 0.85° is consistent with a high-quality texture and a small mosaicity (an instrumental resolution of 0.4° in  $\varphi$  was determined).

### 3.3. Ferroelectric characterization

The ferroelectric behavior of various PYbN-PT films was also studied. Fig. 11 shows the polarization hysteresis loops for two heteroepitaxial 1  $\mu\text{m}$ -thick PYbN-PT thin films with different ceramic target compositions. For the investigated compositions, both heterostructures exhibit well-developed and fairly symmetric hysteresis loops with remanent ( $P_r$ ) and saturation ( $P_s$ ) polarizations as high as 50–60 and 70–80  $\mu\text{C}/\text{cm}^2$ , respectively. The good orientation is quite effective to obtain high remanent polarizations in  $\langle 001 \rangle$ -oriented thin films. It is also possible that the elongation of the lattice constant along the growth direction enhances the ionic displacements somewhat [28]. Indeed, the out-of-plane lattice parameter  $a_{\text{pc}}$  of various heteroepitaxial films, calculated from XRD patterns, is systematically higher than the lattice parameter of conventional polycrystalline PYbN-PT ceramics (Fig. 12). The cause for the correlation between lattice constant extension and the Lotgering factor is not known definitively, though an increase in either bombardment or the degree of biaxial stress may be important. The high values of the polarizations, at least four or five times those obtained in PMN-PT deposited in the same conditions [15], are consistent with the higher transition temperature in the PYbN-PT material. The combination of a high switchable polarization and larger dielectric constant suggests that these materials may have good piezoelectric properties.

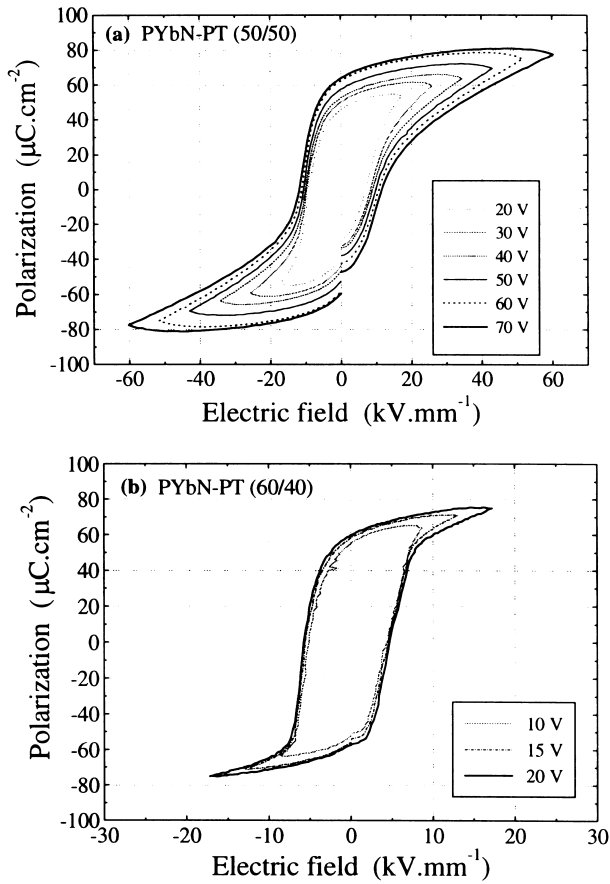


Fig. 11. Polarization hysteresis of heteroepitaxial 1  $\mu\text{m}$ -thick PYbN-PT thin films deposited on SRO / LAO substrates. (a) PYbN-PT (50/50):  $f \sim 16$  Hz;  $P \sim 300$  mTorr;  $T = 620^\circ\text{C}$ ;  $d_{\text{target-substrate}} \sim 5.5$  cm. (b) PYbN-PT (60/40):  $f \sim 16$  Hz;  $P \sim 300$  mTorr;  $T = 655^\circ\text{C}$ ;  $d_{\text{target-substrate}} \sim 5.5$  cm.

#### 4. Conclusion

To the best of the authors' knowledge, this is the first report of heteroepitaxial films of the relaxor-PbTiO<sub>3</sub> solid solution  $\text{Pb}[\text{Yb}_{1/2}\text{Nb}_{1/2}]\text{O}_3$ . Avoiding the occurrence of PbO<sub>x</sub> or pyrochlore phases was found to be very difficult and was only possible in a narrow processing window. High laser frequencies ( $f \geq 14$  Hz) associated with rather high temperatures ( $560 \leq T \leq 660^\circ\text{C}$ ) and high oxygen pressures ( $P \sim 300\text{--}400$  mTorr) favored the perovskite structure. The epitaxial effect of the SrRuO<sub>3</sub> / LaAlO<sub>3</sub> substrates during the growth leads to strongly  $\langle c \rangle$ -oriented PYbN-PT thin films. Off-axis X-ray diffraction  $\varphi$ -scans confirm the good texturation of the heterostructures, pointing out 'pseudo-cube' on 'pseudo-cube' in-plane arrangements. Because of their high ferroelectric activity ( $P_r \sim 50\text{--}60$   $\mu\text{C}/\text{cm}^2$ ), such heterostructures are likely to be promising alternative materials for the fabrication of MEMS devices. Further improvements in the microstructural and electrical properties should be possible by additional optimization of the processing parameters (such as the appropriate choice of wt.% excess PbO in the target or the addition of dopants).

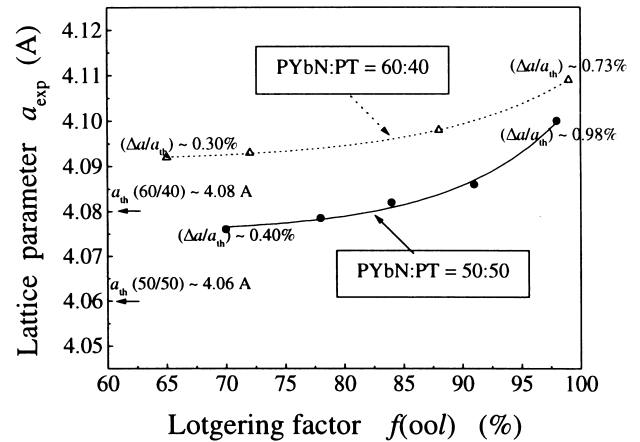


Fig. 12. Lattice parameter  $a_{\text{pc}}$  of heteroepitaxial PYbN-PT thin films deposited on SRO / LAO substrates as a function of thin film crystallization state and ceramic target composition.

#### Acknowledgements

The authors wish to thank B. Jones and M. Angelone for their technical support (target preparation and texture characterization, respectively). This work has been supported by the Office of Naval Research (US) under the project number N00014-98-1-0527. One of the author (V.B.) also acknowledges the DRET/DGA (France) for its financial support under the grant No. 93811113.

#### References

- [1] S. Hirano, T. Yogo, K. Kikuta, K. Kato, W. Sakamoto, S. Ogasahara, *Ceram. Trans. Ferroelectric Films* 25 (1992) 19.
- [2] J.F. Nye, *Physical Properties of Crystals*, Oxford University Press, Oxford, 1979.
- [3] S.E. Park, T.R. Shrout, *MRS Innov.* 1 (1997) 20.
- [4] S.L. Swartz, T.R. Shrout, *MRS Bull.* 17 (1982) 1245.
- [5] S.L. Swartz, T.R. Shrout, W.A. Schulze, L.E. Cross, *J. Am. Ceram. Soc.* 67 (1984) 311.
- [6] T. Kobayashi, S. Shimanuki, S. Saitoh, Y. Yamashita, *Jpn. J. Appl. Phys.* 36 (1997) 6035.
- [7] D.L. Polla, *Micro. Eng.* 29 (1995) 51.
- [8] J.F. Shepard, PhD Thesis, The Pennsylvania State University 1998.
- [9] F. Xu, PhD Thesis, The Pennsylvania State University, 1999.
- [10] Y. Yamashita, N. Ichinose, in: B.M. Kulwicki, A. Amin, A. Safari (Eds.), *International Symposium on Applications of Ferroelectrics*, East Brunswick, NJ, USA, Aug. 18–21, 1996. *Proc. 10th IEEE Int. Symp. Appl. Ferroelectric.* 1 (1996) 71.
- [11] Y. Yamashita, *Jpn. J. Appl. Phys.* 33 (1994) 5328.
- [12] J. Kuwata, K. Uchino, S. Nomura, *Jpn. J. Appl. Phys.* 21 (1982) 1298.
- [13] S.E. Park, T.R. Shrout, *J. Appl. Phys.* 82 (1997) 1804.
- [14] S.-F. Liu, S.-E. Park, T.R. Shrout, L.E. Cross, *J. Appl. Phys.* 85 (1999) 2810.
- [15] J.P. Maria, W. Hackenberger, S. Trolier-Mckinstry, *J. Appl. Phys.* 84 (1998) 5147.
- [16] J.P. Maria, PhD Thesis, The Pennsylvania State University 1998.
- [17] B. Jiang, V. Balu, T. Chen, et al., *Symp. VLSI Technology*, Honolulu, Hawaii, USA, June 11–13, 1996, *VLSI Tech. Dig. Technol. Pap.* (1996) 26.

- [18] T. Nakamura, Y. Nakao, A. Kamisawa, H. Takasu, *Appl. Phys. Lett.* 65 (1994) 1522.
- [19] X.D. Wu, S.R. Foltyn, R.C. Dye, Y. Coulter, R.E. Muenchausen, *Appl. Phys. Lett.* 62 (1993) 2434.
- [20] C.L. Chen, Y. Cao, Z.J. Huang, et al., *Appl. Phys. Lett.* 71 (1997) 1047.
- [21] J.P. Maria, S. Trolier-McKinstry, D.G. Schlom, M.E. Hawley, G.W. Brown, *J. Appl. Phys.* 83 (1998) 4373.
- [22] T. Yamamoto, S. Ohashi, *Jpn. J. Appl. Phys.* 34 (1995) 5349.
- [23] H. Lim, H.J. Kim, W.K. Choo, *Jpn. J. Appl. Phys.* 34 (1995) 5449.
- [24] J.S. Horwitz, D.B. Chrisey, R.M. Stroud, et al., *Appl. Surf. Sci.* 127 (1998) 507.
- [25] D.B. Chrisey, G.K. Hubler, *Pulsed Laser Deposition of Thin Films*, Wiley, New York, 1994.
- [26] S.L. Swartz, T.R. Shrout, *MRS Bull.* 17 (1982) 1245.
- [27] T.R. Shrout, K. Hallial, *Am. Ceram. Soc. Bull.* 66 (1987) 704.
- [28] K. Abe, S. Komatsu, in: B.A. Tuttle, S.B. Desu, R. Ramesh, T. Shio-saki (Eds.), *Ferroelectric Thin Films IV*, Boston, MA, Nov. 29–Dec. 2, 1994. *MRS Symp. Proc.* 361 (1995) 465.